Proceedings of the ASME 2019
International Mechanical Engineering Congress and Exposition
IMECE2019
November 11-14, 2019, Salt Lake City, UT, USA

IMECE2019-10872

SELECTIVE LAMB MODE TRANSMISSION ENABLED BY LOCAL RESONANCE BASED ULTRASONIC METAMATERIAL

Yiran Tian
UM-SJTU Joint Institute
Shanghai Jiao Tong University
Shanghai, China

Yanfeng Shen[1]
UM-SJTU Joint Institute
Shanghai Jiao Tong University
Shanghai, China

ABSTRACT

In this study, a kind of elastic metamaterial substructure was designed for the selective mode filtering and transmission of symmetric and antisymmetric elastic waves. It is composed of double-sided aluminum-lead composite cylinders arranged in a periodic pattern bounded on an aluminum plate. The band structure of elastic metamaterial unit cell is numerically investigated using the modal analysis of a finite element model (FEM) by treating a unit microstructural cell with the Bloch-Floquet boundary condition. Through analyzing the vibration modes of the unit cell, a complete antisymmetric wave bandgap and a complete symmetric wave bandgap can be formed in different frequency ranges. Considering the geometric complexity of the designed substructure, the dynamic effective mass density of the proposed metamaterial unit cell is calculated by considering the structure as a homogeneous medium under the sub-wavelength requirement. The negative effective mass density behavior for in-plane and out-of-plane plate modes will be presented to verify the bandgap effect of different wave modes. A FEM harmonic analysis is further conducted to obtain the spectral response of a chain model and explore the mode filtering efficiency. Finally, a coupled field transient dynamic FEM is carried out to acquire the dynamic response of the structure. The frequency-wavenumber analysis demonstrates the successful achievement of model filtering behavior. The proposed selective mode transmission control methodology possesses great potential in future SHM and NDE applications. A case study for S_0 mode conversion to SH_0 mode using a different metamaterial unit cell is exhibited to illustrate other wave control capabilities. The paper finishes with summary, concluding remarks, and suggestions for future work.

Keywords: metamaterial, mode filtering, structural health monitoring, nondestructive evaluation, mode conversion

1. INTRODUCTION

Guided waves have been investigated as a promising non-destructive testing tool because of their preferred features such as long propagation distance and sensitivity to a variety of structural damage types [1, 2]. However, a precise realization of Lamb waves is generally challenging in the experiments, subjecting to their dispersive and multi modes nature [3]. To overcome the drawbacks, people usually investigate the frequency tuning characteristics, aiming at achieving the single mode excitation [4]. However, this method is limited by a specific frequency and cannot promise to achieve single mode excitation completely.

Recently, many researches have been developed to manipulate the elastic wave modes. Wu et al. indicated a significant amount of mode conversion from transverse waves to longitudinal waves, when proposed metamaterials achieving simultaneously negative effective shear modulus and mass density [5]. Through a carefully designed transmodal elastic metasurface, Kim et al. completed a total mode conversion between longitudinal and shear elastic waves for a broad of incident angles [6]. In the one-dimensional phononic crystal plates, Zhu et al. demonstrated how the unidirectional transmission behavior can be obtained for either antisymmetric waves or symmetric waves [7]. Yan et al. successfully achieved mode conversion for SH guided waves from evanescent into propagating using a semi-analytical approach [8]. The wave and vibration control capabilities of double-sided pillared elastic metamaterials have also been investigated. They can achieve double-negative properties and bandgap enlargement [9, 10]. However, to our best knowledge, the selective mode filtering and transmission behavior for symmetric waves and antisymmetric waves through elastic ultrasonic metamaterials has not been discovered and demonstrated.

[1] Contact author: yanfeng.shen@sjtu.edu.cn

This paper focuses on applying wave and vibration control methodologies on Structural Health Monitoring (SHM) and Non-destructive Evaluation (NDE) applications. In this research, an elastic metamaterial substructure comprised of double-sided aluminum-lead composite cylinders is proposed to realize the selective mode filtering and transmission behavior for symmetric elastic waves (S waves) and antisymmetric elastic waves (A waves). Through investigating the spectral bandgap effect for different wave modes, this work strives to put forward a new aspect for implementing the single-mode excitation, assisting to improve the accuracy and efficiency for SHM and NDE applications. This paper starts with analyzing the band structure of a unit metamaterial substructure. Through investigating different vibration modes, a complete S waves bandgap and a complete A waves bandgap are formed. Then the frequency spectrum of a chain FEM will be further conducted through harmonic analysis to explore the bandgaps efficiency. Finally, a case study is further presented with elastic waves propagating in two host plates with and without metamaterials substructures. The frequency-wavenumber analysis shows the successful realization of the selective mode filtering behavior.

2. BAND STRUCTURE OF A UNIT ULTRASONIC METAMATERIAL CELL

Figure 1a shows the schematic diagram of a unit ultrasonic metamaterial cell. It is constructed by a 2-mm thick aluminum plate and a double-sided aluminum-lead composite cylinder bounded on the plate. The radius r of the stubs is 1.75-mm and the lattice constant a of the unit cell is 5 mm. The heights of aluminum and lead cylinders are separately 3 mm and 2.5 mm. These parameters are satisfied with the sub-wavelength requirement. Then the standard finite element method is applied for a case study, simulating a harmonic wave propagating into a periodic material. By periodic, it is here meant that the material can be divided into finite-sized identical, so-called periodic cells [11]. Thus, one unit cell can represent the entire structure. By treating a unit cell with Bloch-Floquet boundary condition (Figure 1b), the standard finite element codes for computation of band structure of ultrasonic metamaterials are conducted in ANSYS 15.0 package. As shown in Figure 1c, a complete bandgap ranging from 98.52-118.8 kHz is opened up due to the strong interaction between the guided waves and the double-sided cylinders. Based on the locally resonance (LR) mechanism [12], when the excitation frequency approaches to the resonant frequency of the meta-surface structure, the corresponding frequency will not be shown in the dispersion curve. Meanwhile, it means the guided waves under this frequency cannot pass through the structure and bandgaps develop.

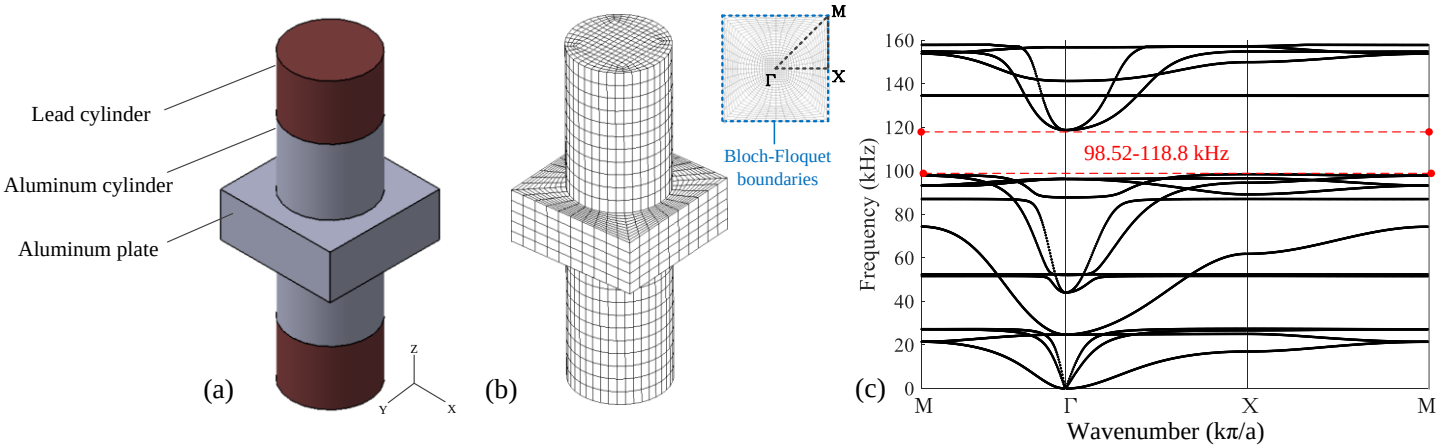

FIGURE 1: (a) METAMATERIAL UNIT CELL SCHEMATIC DIAGRAM; (b) METAMATERIAL UNIT CELL FINITE ELEMENT MODEL; (c) BAND STRUCTURE OF THE METAMATERIAL UNIT CELL

3. MECHANISM INVESTIGATION FOR A WAVES AND S WAVES BANDGAPS FORMATION

3.1 Modal Analysis of Unit Cell Model

To comprehend the mechanism behind the formation of A waves and S waves bandgaps, the dispersion curve along ΓX direction, which is parallel to the propagation of the excitation waves, is zoomed in to investigate different vibration modes of the unit substructure, as shown in Figure 2a. Figure 2b demonstrates the displacement fields of the unit substructure for particular resonant modes: α, β located in X point. After a closer look into the vibrational motion of the composite cylinders, mainly two kinds of resonant modes can be picked out in the case: the lateral anti-symmetric vibrational motion and the lateral symmetric motion. From Figure 2b, in the first row, it contains the anti-resonance (α) followed by the degenerate resonance (α'). In this vibration mode, two composite cylinders vibrate to the opposite directions and the displacement fields of them show the same absolute value but inverse signs, contributing to the zero displacement distribution in the host plate. Thus, the transmission of the A waves will become prevented in the plate, resulting in a

complete A waves bandgap ranging from 17.04 to 24.82 kHz. The same mechanism can be explained for S waves. From the second row, in symmetric resonant modes, two composite cylinders vibrate to the same direction and the displacement distribution in them have the same absolute value and sign, giving rise to the zero displacement amplitude of the host plate. Then the propagation of the symmetric waves in the plate will be prohibited, forming a complete S waves bandgap covering from 27.48 to 44.15 kHz.

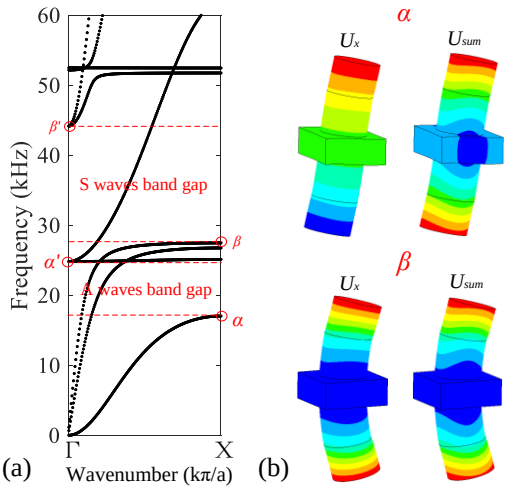

FIGURE 2: (a) THE ZOOMED-IN DISPERSION CURVE ALONG ΓX DIRECTION; (b) THE DISPLACEMENT FIELDS OF THE METAMATERIAL SUBSTRUCTURE FOR PARTICULAR RESONANT MODES

3.2 Dynamic Effective Mass Density Calculation of Unit Cell Model

Knowing the dynamic effective properties of the elastic metamaterials is necessary for studying their wave propagation characteristics. Due to the geometrical complexity, a numerical-based effective medium method is employed under the sub-wavelength condition. Zhu et al. elaborately demonstrated the calculation process of the dynamic effective mass density by treating the structure as a homogeneous medium [13]. After applying a local harmonic displacement distribution on the surrounding boundaries, the global resultant force on each boundary can be obtained through the integration of the corresponding average stresses. Figure 4 shows the results comparison between the dispersion curve along ΓX direction and the normalized dynamic effective mass density plot. Figure 4b exhibits the negative effective mass density tendency, i.e., ρ11 (blue solid line) for in-plane waves. It is worth mentioning that the normalized effective mass density along x and y directions (ρ11 and ρ22) show the same trend considering the geometry symmetric of the unit cell. From the result, it can be observed that the normalized effective mass density ρ11 become negative within the S waves bandgap and the complete bandgap. The same phenomena can be presented in the normalized effective mass density for out-of-plane waves. An out-of-plane waves bandgap ranging from 98.25-141.3 kHz, covering the complete bandgap, can be distinguished from the plot (which will be shown in the presentation and journal paper). The physical mechanism behind the formation of the out-of-plane waves bandgap is similar with A waves and S waves bandgaps discussed before.

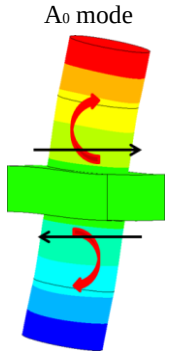

FIGURE 3: THE VIBRATION MODE FOR ANTI-RESONANCE MOTION

It can be noticed that no negative effective mass density ranges appear within the A waves bandgap. The reason behind it can be explained by the anti-resonance motion, as shown in Figure 3. The resultant force is equal to zero due to the same amplitude and opposite directions of the two traction forces. Although the resultant moment is not equal to zero, the bending resonance will not interact with the motion in the plate and contribute to the negative mass density. Thus, ρ11 and ρ22 will not become negative around the A waves bandgap [10].

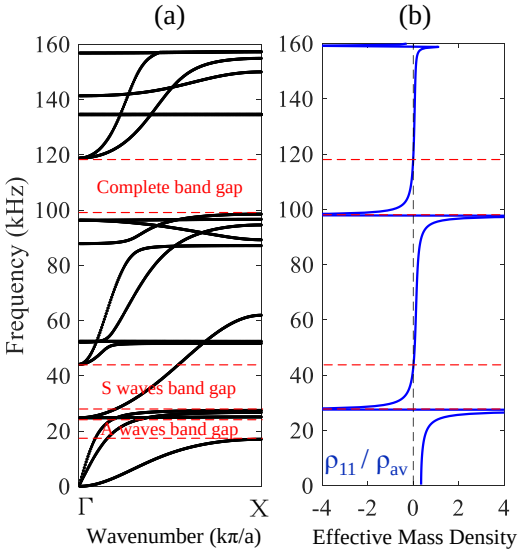

FIGURE 4: (a) THE DISPERSION RELATION OF THE UNIT CELL ALONG ΓX DIRECTION; (b) THE FREQUENCY SPECTRA OF THE NORMALIZED DYNAMIC EFFECTIVE MASS DENSITY: ρ_{11}/ρ_{av}

4. SPECTRAL RESPONSE OF FINITE ELEMENT MODELING

4.1 Harmonic Analysis of Unit Cell Chain Model

Harmonic analysis was conducted to probe the selective mode filtering efficiency. The metamaterial plate is constructed by an array of 10×1 unit cells (Figure 1a) bounded on the surface, as shown in Figure 5. A 50-N external force sweeping from 0 to 50 kHz was applied on the top surface of the structure to excite an incident wave containing both A_0 and S_0 modes propagating into the plate along the x direction. The objective of constructing the model is to obtain the in-plane and out-of-plane displacements of sensing points m and n, which are on the top and bottom surfaces of the plate, as well as equivalent stress responses of the whole structure under the excitation at different frequencies. The in-plane displacement is used to extract the S_0 mode component, and out-of-plane displacement is for A_0 mode extraction. Two non-reflective boundaries (NRB) [14] were added on both ends of the plate to absorb the boundary reflections. The square area is zoomed in to show the detailed equivalent stress responses of the structure at different excitation frequencies.

4.2 Mode Extraction from Displacement Responses

Figure 6 shows the frequency spectrum of the metamaterial plate from harmonic analysis. It can be observed that a complete A_0 mode waves bandgap (red dash line within red square area) ranging from 17 to 24.5 kHz and a complete S_0 mode waves bandgap (blue solid line within blue square area) covering from 27.5 to 38 kHz are formed in two separate ranges. To illustrate the extraordinary effect of the metamaterial substructures, the equivalent stress of the structure is also plotted. Three fundamental frequencies were calculated to show the equivalent stress of the structure, which are 10 kHz, 20 kHz and 28 kHz. When the excitation frequency is 10 kHz without two bandgaps, both A_0 and S_0 mode waves can propagate into the plate after passing through the metamaterial area. By contrast, 20 kHz is the frequency within the A_0 bandgap. After passing through the metamaterial structures, the propagating waves only contain the S_0 mode. The last several composite cylinders vibrate in the symmetric resonance. And similarly, the same behavior can be verified when the incident wave was excited at 28 kHz within the S_0 bandgap. The propagating waves passing through the metamaterial area only leave the A_0 mode. The last few composite stubs vibrate in anti-symmetric resonance. Continuing work is being conducted, the key results will be presented at the conference.

Above all, the results from the harmonic analysis agree well with the bandgap feature in modal analysis. The small differences between them come from the finite unit cell number. The selective mode filtering and transmission phenomenon can be verified through harmonic analysis.

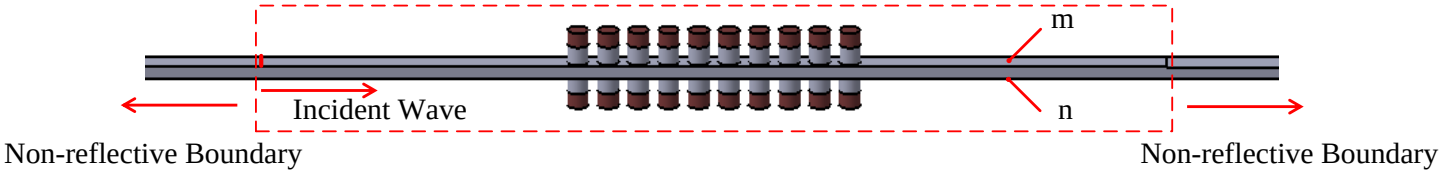

FIGURE 5: MODEL LAYOUT OF A 10×1 UNIT CELLS CHAIN MODEL IN HARMONIC ANALYSIS

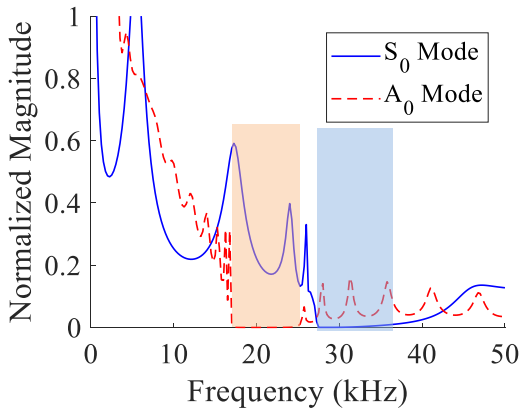

FIGURE 6: THE EQUIVALENT STRESS AND DISPLACEMENT RESULTS FROM HARMONIC ANALYSIS: (a) THE FREQUENCY SPECTRUM OF A_0 AND S_0 MODES; (b) EQUIVALENT STRESS RESPONSES OF THE STRUCTURE UNDER 10 kHz, 20 kHz, AND 28 kHz

5. FREQUENCY-WAVENUMBER RESPONSE OF FINITE ELEMENT MODELING

5.1 Transient Dynamic Analysis of Unit Cell Chain Model

Figure 8 shows the model layouts of a pitch-catch NDE procedure for a homogeneous aluminum plate and a metamaterial plate. One 5-mm×5-mm×0.2-mm rectangular Piezoelectric Wafer Active Sensor (PWAS) was bounded on the left side of each plate to generate guided waves. The in-plane displacement response along x direction of the points within the sensing area is extracted out for frequency-wavenumber analysis. For the metamaterial plate, an array of 10×1 double-sided aluminum-lead composite cylinders was bounded on the homogeneous aluminum plate. Non-reflective boundaries (NRB) were implemented on both ends of the plates to avoid the influence from boundary reflections. The transmitter PWAS would generate a 100 voltage peak-to-peak (vpp) 20-count Hamming-windowed tone burst signal with the central frequency 10 kHz, 20 kHz, and 28 kHz separately. The waves would propagate through the metamaterial area, achieving the selective mode filtering and transmission behavior for 20 kHz excitation within A_0 bandgap and 28 kHz excitation within S_0 bandgap. PWAS transducers were modeled with the couple field elements (SOLID5), which enable to couple the electrical and mechanical variables. The three-dimensional structure was modeled with four-node structural element SOLID45. To ensure the accuracy of the results and solve the problem more efficiently, the element size and time step should be optimized. After the calculation, in our model the maximum element size was set to be 0.5-mm to guarantee the space discretization requirement; the time-step was set to be 2-μm.

5.2 Frequency-Wavenumber Response

Figure 7 shows the frequency-wavenumber responses of a 10×1 unit cells metamaterial plate and a homogeneous aluminum plate. It can be observed that when the excitation frequency is 10 kHz without any bandgaps, the guided waves propagating through the sensing area contain both A_0 and S_0 wave modes in both plates. However, when the incident wave is excited at 20 kHz within the A_0 bandgap, A_0 mode waves are filtered away by the metamaterial substructures, only S_0 mode waves can pass through. Similarly, the S_0 mode waves cannot propagate through the metamaterial area at 28 kHz excitation frequency within the S_0 bandgap. Contrast that with the homogeneous plate, the selective mode filtering and transmission behavior cannot be seen. The proposed metamaterial substructure has the ability of achieving the single mode excitation, which will improve the applications of the SHM and NDE.

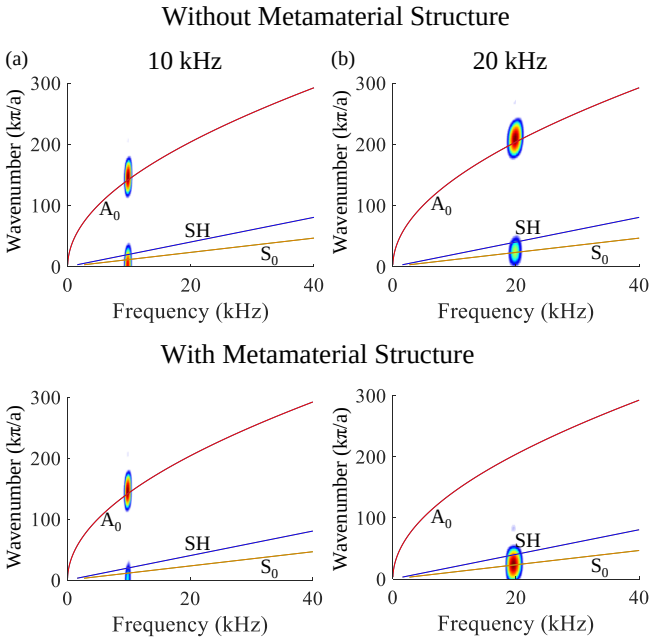

FIGURE 7: FREQUENCY-WAVENUMBER RESPONSES OF A 10×1 UNIT CELLS METAMATERIAL PLATE AND A HOMOGENEOUS ALUMINUM PLATE AT DIFFERENT EXCITATION FREQUENCIES: (a) 10 kHz (WITHOUT ANY BANDGAPS); (b) 20 kHz (WITHIN A_0 BANDGAP)

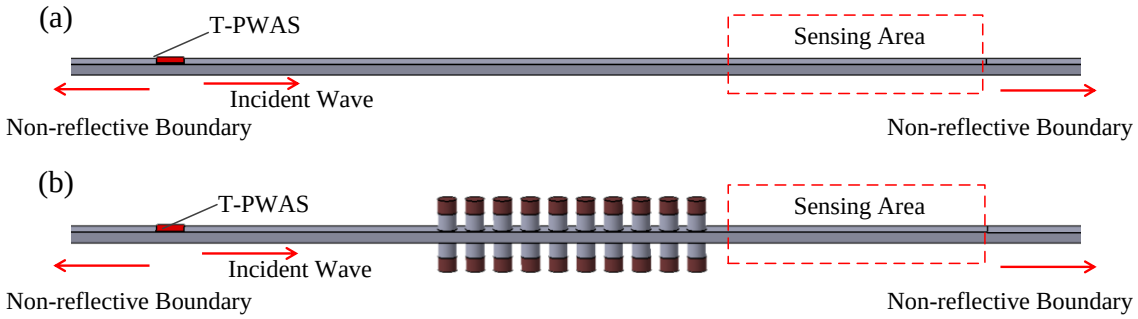

FIGURE 8: MODEL LAYOUT OF A 10×1 UNIT CELLS CHAIN MODEL IN COUPLED FILED TRANSIENT DYNAMIC ANALYSIS

6. CASE STUDY FOR S_0 MODE CONVERSION TO SH_0 MODE BY ULTRASONIC METAMATERIAL

Based on the discussed mechanism behind the formation of a complete A waves bandgap and a complete S waves bandgap (Figure 2), a case study for S_0 mode conversion to SH_0 mode through a different carefully designed ultrasonic metamaterial substructure was illustrated in this section. Figure 9a shows the FEM of the metamaterial unit cell. It is constructed by an aluminum-polylactic acid (PLA) composite cylinder bounded on a hollowed aluminum host plate. The height of the aluminum stub L is 3-mm, and the height of the PLA stub is l 1-mm. The lattice constant a of the unit cell is 10-mm. This kind of design has the ability of achieving the mode conversion and mode filtering behavior at the same time. The hollowed host plate can complete the mode conversion from S_0 mode to SH_0 mode. And the bounded composite cylinder can achieve the selective mode filtering behavior for S_0 mode. After applying Bloch-Floquet constraints on the boundaries, the dispersion curve along ΓX direction can be calculated numerically and shown in Figure 9c. Figure 9d presents the frequency spectrum of the metamaterial plate, which is similar with the structure shown in Figure 5, through the harmonic analysis. The external force along x positive direction was applied on the top and bottom surfaces of the plate simultaneously to generate S_0 mode excitation. By comparing the results from the modal analysis and harmonic analysis, a complete mode conversion bandgap ranging from 37.75 to 42 kHz for S_0 to SH_0 can be obviously observed. A displacement distribution of the particular mode γ around 40 kHz in modal analysis was displaced in Figure 9b. It can be observed that the magnitude of displacement along x direction is almost zero in the host aluminum plate. However, the magnitude of the displacement along y direction cannot be ignored. And it is worthy mentioning that the whole structure vibrates along y direction, that is, only SH_0 mode wave can transmit through the metamaterial area and propagate in the plate. Continuing work is being conducted. The key results will be published in a journal paper.

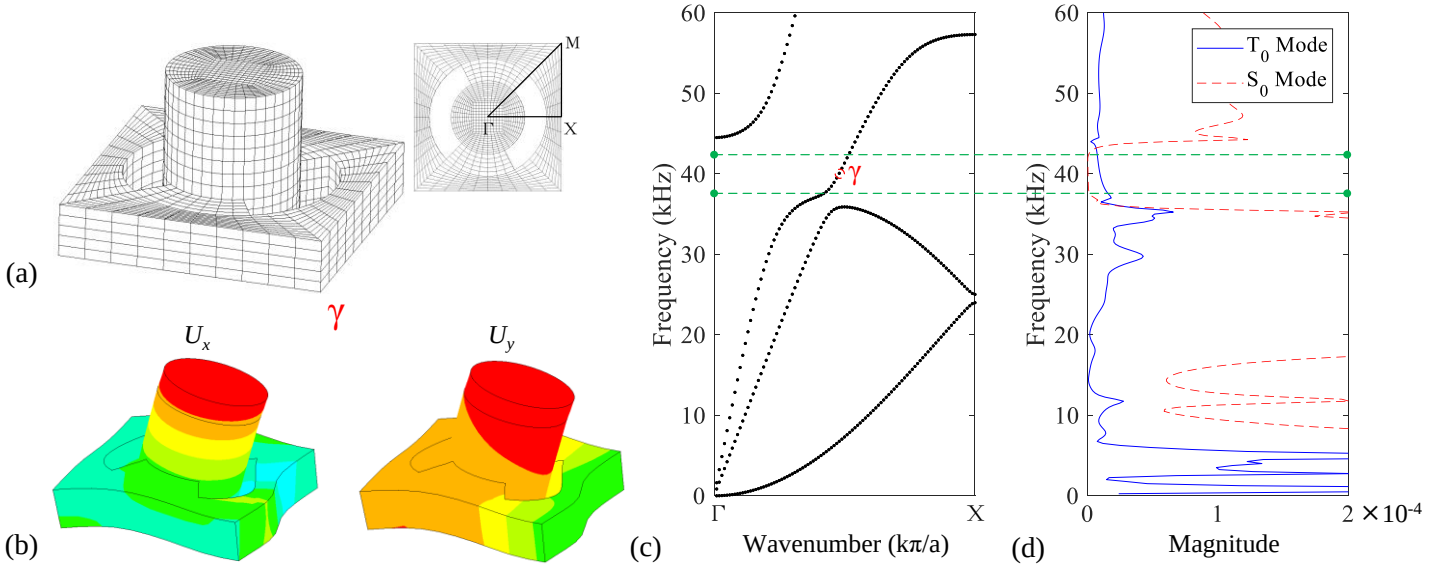

FIGURE 9: (a) FEM OF METAMATERIAL SUBSTRUCTURE; (b) DISPLACEMENT DISTRIBUTION ALONG X AND Y DIRECTIONS FOR RESONANT MODE γ; (c) DISPERSION CURVE ALONG ΓX DIRECTION; (d) FREQUENCY SPECTRUM OF THE METAMATERIAL PLATE

7. CONCLUDING REMARKS

In this paper, a selective mode transmission control methodology of using metamaterial for the improvement of SHM and NDE applications was put forward. A metamaterial substructure was designed with double-sided aluminum-lead composite cylinders. This kind of metamaterial can achieve a complete antisymmetric wave bandgap and a complete symmetric wave bandgap in different frequency ranges. Through treating a unit cell with the Bloch-Floquet boundary condition, the band structure of the unit cell is numerically investigated using the modal analysis. The dynamic effective mass density behavior for in-plane and out-of-plane modes is calculated by considering the structure as a homogeneous medium under the sub-wavelength condition. The negative effective properties are consistent with bandgap effect. A FEM harmonic analysis is further conducted to obtain the spectral response of a chain model and explore the mode filtering efficiency. Ultimately, a coupled field transient dynamic FEM is conducted to obtain the dynamic response of the structure. The frequency-wavenumber analysis demonstrates the successful achievement of selective mode filtering and transmission behavior. And other wave control capability such as mode conversion for S_0 mode to SH_0 mode can also be achieved through carefully designed ultrasonic metamaterial unit cell. The proposed method processes great potential in future SHM and NDE applications.

ACKNOWLEDGMENTS

The support from the National Natural Science Foundation of China (contract number 51605284) is thankfully acknowledged.

REFERENCES

[1] Giurgiutiu V., "Tuned Lamb Wave Excitation and Detection with Piezoelectric Wafer Active Sensors for Structural Health Monitoring," *Journal of Intelligent Material Systems and Structures*, vol. 16, no. 4, pp. 291-305, 2016

[2] Raghavan A. and Cesnik S. E. C., "Finite-dimensional piezoelectric transducer modeling for guided wave based structural health monitoring," *Smart Materials and Structures*, vol. 14, no. 6, pp. 1448-1461, 2005

[3] Deng M., Wang P., and Lv X., "Experimental verification of cumulative growth effect of second harmonics of Lamb wave propagation in an elastic plate," *Applied Physics Letters*, vol. 86, no. 12, 2005

[4] Shen Y. and Giurgiutiu V., "WaveFormRevealer: An analytical framework and predictive tool for the simulation of multi-modal guided wave propagation and interaction with damage," *Structural Health Monitoring: An International Journal*, vol. 13, no. 5, pp. 491-511, 2014

[5] Wu Y., Lai Y., and Zhang Z. Q., "Elastic metamaterials with simultaneously negative effective shear modulus and mass density," *Phys Rev Lett*, vol. 107, no. 10, p. 105506, Sep 2 2011

[6] Kim M. S., Lee W. R., Kim Y. Y., and Oh J. H., "Transmodal elastic metasurface for broad angle total mode conversion," *Applied Physics Letters*, vol. 112, no. 24, 2018

[7] Zhu X., Zou X., Liang B., and Cheng J., "One-way mode transmission in one-dimensional phononic crystal plates," *Journal of Applied Physics*, vol. 108, no. 12, 2010

[8] Yan X. and Yuan F. G., "A semi-analytical approach for SH guided wave mode conversion from evanescent into propagating," *Ultrasonics*, vol. 84, pp. 430-437, Mar 2018

[9] Assouar M. B. and Oudich M., "Enlargement of a locally resonant sonic band gap by using double-sides stubbed phononic plates," *Applied Physics Letters*, vol. 100, no. 12, 2012

[10] Wang W., Bonello B., Djafari-Rouhani B., Pennec Y., and Zhao J., "Double-Negative Pillared Elastic Metamaterial," *Physical Review Applied*, vol. 10, no. 6, 2018

[11] Åberg M. and Gudmundson P., "The usage of standard finite element codes for computation of dispersion relations in materials with periodic microstructure," *The Journal of the Acoustical Society of America*, vol. 102, no. 4, pp. 2007-2013, 1997

[12] Zhu R., Liu X. N., Hu G. K., Yuan F. G., and Huang G. L., "Microstructural designs of plate-type elastic metamaterial and their potential applications: a review," *International Journal of Smart and Nano Materials*, vol. 6, no. 1, pp. 14-40, 2015

[13] Zhu R., Liu X. N., Huang G. L., Huang H. H., and Sun C. T., "Microstructural design and experimental validation of elastic metamaterial plates with anisotropic mass density," *Physical Review B*, vol. 86, no. 14, 2012

[14] Shen Y. and Giurgiutiu V., "Effective non-reflective boundary for Lamb waves: Theory, finite element implementation, and applications," *Wave Motion*, vol. 58, pp. 22-41, 2015